ELSEVIER

Comput. Methods Appl. Mech. Engrg. 190 (2001) 6895–6908

Computer methods in applied mechanics and engineering

www.elsevier.com/locate/cma

Adaptive mixed finite element method for Reissner–Mindlin plate

C. Carstensen [a,*], K. Weinberg [b]

[a] *Mathematisches Seminar, Christian-Albrechts-Universität zu Kiel, Ludewig-Meyn-Str. 4, D-24098 Kiel, Germany*
[b] *Graduate Aeronautical Laboratories, California Institute of Technology, Pasadena, CA 91125, USA*

Received 1 March 2000; received in revised form 7 June 2001

Abstract

Mixed finite element methods are designed to overcome shear locking phenomena observed in the numerical treatment of Reissner–Mindlin plate models. Automatic adaptive mesh-refining algorithms are an important tool to improve the approximation behavior of the finite element discretization. In this paper, a reliable and robust residual-based a posteriori error estimate is derived, which evaluates a t-depending residual norm based on results in [D. Arnold, R. Falk, R. Winther, Math. Modell. Numer. Anal. 31 (1997) 517–557]. The localized error indicators suggest an adaptive algorithm for automatic mesh refinement. Numerical examples prove that the new scheme is efficient. © 2001 Elsevier Science B.V. All rights reserved.

Keywords: Mixed finite element methods; Reissner–Mindlin plate; Shear locking; Reliability; A posteriori error estimates; Adaptive algorithm

1. Introduction

Mixed finite element schemes in general require deeper mathematical analysis as an arbitrary choice of ansatz and test spaces yields instabilities. Very recently, new finite element methods were introduced in the mathematical literature [1,3,4,11,13] for the effective numerical treatment of the Reissner–Mindlin model of the moderately thick plate

$$\frac{t^2}{6}\operatorname{div}\left(\frac{\nu}{1-\nu}\,\mathbb{I}\operatorname{div}\vartheta+\varepsilon(\vartheta)\right)+(\nabla w-\vartheta)=0, \tag{1.1}$$

$$\operatorname{div}(\nabla w-\vartheta)+kf=0. \tag{1.2}$$

Therein, a new parameter α stabilizes the finite element discretization. In this paper, we derive a reliable residual-based a posteriori error estimate for those and the classical conforming Reissner–Mindlin plate models. For the exact resp. finite element solution (ϑ,w,γ) resp. $(\vartheta_h,w_h,\gamma_h)$ to (1.1) and (1.2), we derive an upper bound for the error

$$\|(\vartheta-\vartheta_h,w-w_h)\|_{H_0^1(\Omega)}+\|\gamma-\gamma_h+\alpha(\vartheta-\vartheta_h-\nabla(w-w_h))\|_{H^{-1}(\operatorname{div})\cap t\cdot L^2}, \tag{1.3}$$

* Corresponding author. Current address: Institute for Applied Mathematics and Numerical Analysis, Vienna University of Technology, Wiedner Hanptstrasse 8–10, A-1040 Vienna, Austria.

E-mail addresses: carsten.carstensen@tuwien.ac.at (C. Carstensen), weinberg@aero.caltech.edu (K. Weinberg).

PII: S0045-7825(01)00268-7

where $\vartheta - \vartheta_h$ is the error of the rotations, $w - w_h$ is the error of the displacement and $\gamma - \gamma_h + \alpha(\vartheta - \vartheta_h - \nabla(w - w_h))$ is the shear stress error. The upper bound requires standard techniques in the proofs of a posteriori error estimates [17] plus an estimate of a global norm of $\rho := (1 - \alpha t^2)(\vartheta_h - \nabla w_h) - t^2\gamma_h$ which is defined over an extremal global additive split $\rho_1 + \rho_2 = \rho$. The localization of this term requires an estimate from [7] based on a deeper result due to Tartar. The resulting upper bound to (1.3) reads $c_1\eta_{\mathscr{T}}$, where the error estimate $\eta_{\mathscr{T}}$ is

$$\eta_{\mathscr{T}}^2 := \sum_{T\in\mathscr{T}} \eta_T^2. \tag{1.4}$$

The point is that the positive constant c_1 neither depends on right-hand sides, exact and discrete solutions, on α, nor on the thickness t. However, the question of the converse estimate (up to higher-order contributions), called efficiency estimate [17], is affirmatively answered for a few of the terms behind (1.4) and left open for the term $\rho_1 + \rho_2 = \rho$.

It appears an interesting mathematical problem to find norms and finite element schemes in which reliable and efficient a posteriori error estimates exist; we refer to [8,12] for the recent progress. The purpose of this paper is to derive robust reliable estimates for a huge class of conforming finite element discretizations under minimal assumptions in h-independent norms, and to express them in locally computable terms. Then we employ the corresponding local error indicators η_T in (1.4) to control an adaptive algorithm for automatic mesh refinement. Typical numerical examples prove the excellent performance of our new adaptive finite element scheme.

The remaining part of the paper is organized as follows. The weak formulation and the conforming finite element discretization of (1.1) and (1.2) as well as certain (non-standard) norms and Sobolev spaces are recalled from the literature in Section 2. The main result and the necessary notation for (1.4) will be given in Section 3 where we also propose our adaptive algorithm. In Section 4 we compare our error estimate with the exact value of (1.3) given by an analytical solution and we demonstrate with further examples the superiority of automatically generated meshes. Details of the mathematical proof in Section 5 conclude this work.

2. Mixed formulation and finite element discretization

The weak form of the Reissner–Mindlin plate model is rewritten with bilinear forms:

$$a(\vartheta, w; \varphi, v) := \int_\Omega \varepsilon(\vartheta) : \mathbb{C}\varepsilon(\varphi)\,\mathrm{d}x + \int_\Omega \alpha(\vartheta - \nabla w)\cdot(\varphi - \nabla v)\,\mathrm{d}x, \tag{2.1}$$

$$b(\vartheta, w; \eta) := \int_\Omega (\vartheta - \nabla w)\cdot\eta\,\mathrm{d}x, \tag{2.2}$$

$$c(\gamma; \eta) := \int_\Omega \beta\gamma\cdot\eta\,\mathrm{d}x \tag{2.3}$$

for $\vartheta, \varphi \in H_0^1(\Omega)^2$, $v, w \in H_0^1(\Omega)$, and $\gamma, \eta \in L^2(\Omega)^2$. The elasticity operator $\mathbb{C}$ is defined by

$$\mathbb{C}\tau = \frac{1}{6k}\left[\tau + \frac{\nu}{1-\nu}\ \mathrm{tr}(\tau)\,\mathbb{I}\right],$$

where $\mathrm{tr}(\tau)$ denotes the trace of $\tau \in \mathbb{R}^{2\times 2}$, ν is the Poisson ratio, and $k = 5/6$ the shear correction factor of the elastic plate. The linear Green strain ε is the symmetric gradient $\varepsilon(\vartheta) := \mathrm{sym}D\vartheta = (\frac{1}{2}(\partial\vartheta_j/\partial x_k + \partial\vartheta_k/\partial x_j))_{j,k=1,2}$. Here and below $f \in L^2(\Omega)$ is an applied force which is already scaled by a factor $Ekt^3/(2(1+\nu))$, E is the Young modulus.

The critical parameter is the small thickness $t > 0$ of the plate which enters (2.1)–(2.3) through $\beta := 1/(t^{-2} - \alpha)$, where α is a parameter with $0 \leqslant \alpha < t^{-2}$ to stabilize the discretization. The classical model is included for $\alpha = 0$ in the *continuous problem: Find* $(\vartheta, w, \gamma) \in H_0^1(\Omega)^2 \times H_0^1(\Omega) \times L^2(\Omega)$ *that satisfies, for all* $(\varphi, v, \eta) \in H_0^1(\Omega)^2 \times H_0^1(\Omega) \times L^2(\Omega)^2$,

$$a(\vartheta, w; \varphi, v) + b(\varphi, v; \gamma) = \int_\Omega fv \,\mathrm{d}x, \tag{2.4}$$

$$b(\vartheta, w; \eta) - c(\gamma; \eta) = 0. \tag{2.5}$$

Here, $L^2(\Omega)$ and $H^1(\Omega)$ denote the usual Lebesgue and Sobolev spaces [5] and $H^1_0(\Omega)$ is the sub-space of all functions with zero boundary values and with dual space $H^{-1}(\Omega)$. The mathematical analysis in [6] shows that, in the limit $t \to 0$ and for $\alpha = 0$, the natural space for the shear variable $\gamma = (t^{-2} - \alpha)(\vartheta - \nabla w)$ is *not* $L^2(\Omega)$ but $H^{-1}(\mathrm{div}; \Omega)$. The space $H^{-1}(\mathrm{div}; \Omega)$ consists of all $\gamma \in H^{-1}(\Omega)^2$ with $\mathrm{div}\,\gamma \in H^{-1}(\Omega)$. Its dual space is

$$H^{-1}(\mathrm{div}; \Omega)^* = H_0(\mathrm{rot}; \Omega) := \{\eta \in L^2(\Omega)^2 : \mathrm{rot}\,\eta \in L^2(\Omega),\ \eta \cdot s = 0 \text{ on } \partial\Omega\}, \tag{2.6}$$

where s is the tangential vector (perpendicular to the exterior unit normal n) along the boundary and $\eta \cdot s$ denotes the tangential trace of η (which is defined in a weak sense by integration by parts). The norms are defined with

$$\|\gamma\|_{H^{-1}(\mathrm{div};\Omega)} := \left(\|\gamma\|^2_{H^{-1}(\Omega)} + \|\mathrm{div}\,\gamma\|^2_{H^{-1}(\Omega)}\right)^{1/2}, \tag{2.7}$$

$$\|\eta\|_{H_0(\mathrm{rot};\Omega)} := \left(\|\eta\|^2_{L^2(\Omega)} + \|\mathrm{rot}\,\eta\|^2_{L^2(\Omega)}\right)^{1/2}. \tag{2.8}$$

Note, if the plate thickness tend towards zero, the solution of (2.4) and (2.5) in $H^1_0(\Omega)^2 \times H^1_0(\Omega) \times H^{-1}(\mathrm{div}; \Omega)$ converges to the solution of the Kirchhoff plate model. However, for a very small but finite thickness $t > 0$, it appears reasonable to consider t-depending norms defined by

$$\|\gamma\|^2_{H^{-1}(\mathrm{div})\cap t\cdot L^2} := \|\gamma\|^2_{H^{-1}(\mathrm{div};\Omega)} + t^2\|\gamma\|^2_{L^2(\Omega)}, \tag{2.9}$$

$$\|\eta\|^2_{H_0(\mathrm{rot})+t^{-1}\cdot L^2} := \inf_{\eta=\eta_1+\eta_2}\left(\|\eta_1\|^2_{H_0(\mathrm{rot};\Omega)} + t^{-2}\|\eta_2\|^2_{L^2(\Omega)}\right). \tag{2.10}$$

The finite element discretization of (2.1)–(2.3) considers discrete sub-spaces $V_h \times W_h \times \Gamma_h$ of $H^1_0(\Omega)^2 \times H^1_0(\Omega) \times L^2(\Omega)$. Thus the *discrete problem* reads: *Find* $(\vartheta_h, w_h, \gamma_h) \in V_h \times W_h \times \Gamma_h$ *that satisfies*, *for all* $(\phi_h, v_h, \eta_h) \in V_h \times W_h \times \Gamma_h$,

$$a(\vartheta_h, w_h; \phi_h, v_h) + b(\phi_h, v_h; \gamma_h) = \int_\Omega fv_h \,\mathrm{d}x, \tag{2.11}$$

$$b(\vartheta_h, w_h; \eta_h) - c(\gamma_h; \eta_h) = 0. \tag{2.12}$$

The discrete spaces $V_h \times W_h \times \Gamma_h$ are $\mathscr{T}$-piecewise polynomials (the index h may refer to the mesh-size of $\mathscr{T}$ but we neglect further sub-indices such as in $\mathscr{T}_h$, α_h, etc.) based on a regular triangulation $\mathscr{T}$ of Ω (cf. [5]). Given $\mathscr{T}$, $\mathscr{P}_k(\mathscr{T})$ denotes the linear space of $\mathscr{T}$-piecewise polynomials of degree $\leqslant k$. Let $\mathscr{S}_k(\mathscr{T})$ denote the continuous discrete functions in $\mathscr{P}_k(\mathscr{T})$ with homogeneous boundary values, i.e.,

$$\mathscr{P}_k(\mathscr{T}) := \left\{\gamma_h \in L^2(\Omega) : \forall T \in \mathscr{T},\ \gamma_h|_T \in \mathscr{P}_k(T)\right\} \quad \text{and} \quad \mathscr{S}_k(\mathscr{T}) := \mathscr{P}_k(\mathscr{T}) \cap H^1_0(\Omega), \tag{2.13}$$

where $\mathscr{P}_k(\omega)$ denotes the vector space of algebraic polynomials of degree $\leqslant k$ regarded as mappings on the domain $\omega \subset \mathbb{R}^2$: if $T \in \mathscr{T}$ is a triangle, $\mathscr{P}_k(T)$ denotes the space of polynomials of total degree $\leqslant k$; while $\mathscr{P}_k(T)$ denotes the space of polynomials of partial degree $\leqslant k$ if T is a parallelogram.

In [13] it is shown that for any non-negative integer k, the discrete space

$$V_h \times W_h \times \Gamma_h = \mathscr{S}_{k+2}(\mathscr{T})^2 \times \mathscr{S}_{k+2}(\mathscr{T}) \times \mathscr{P}_k(\mathscr{T}) \tag{2.14}$$

leads to a stable scheme. Moreover, an a priori error estimate is presented which is quasi-optimal in the sense that there exists a positive constant c_2 (which depends on Ω, k, α, and on the shape of the elements but is independent of their sizes h and of the plate thickness t) such that the discrete problem has a unique solution $(\vartheta_h, w_h, \gamma_h)$ and, with the exact solution (ϑ, w, γ), there holds

$$\begin{aligned}&\|\vartheta-\vartheta_h\|_{H_0^1(\Omega)}+\|w-w_h\|_{H_0^1(\Omega)}+\|\gamma-\gamma_h\|_{H^{-1}(\mathrm{div})\cap t\cdot L^2}\\&\quad\leqslant c_2\left(\inf_{\phi_h\in V_h}\|\vartheta-\phi_h\|_{H_0^1(\Omega)}+\inf_{v_h\in W_h}\|w-v_h\|_{H_0^1(\Omega)}+\inf_{\eta_h\in\Gamma_h}\|\gamma-\eta_h\|_{H^{-1}(\mathrm{div})\cap t\cdot L^2}\right).\end{aligned}\tag{2.15}$$

Note, the L^2-norm of the shear error has the thickness t as a weight in order to result in a t-independent constant c_2. In case of (2.14) and a smooth continuous solution, the poor approximation of the shear yields a convergence order $\mathrm{O}(h^{k+1})$, where h denotes the maximal mesh-size in $\mathscr{T}$. Since the approximation errors of the remaining two best-approximation errors are of higher order, a subtle choice of the parameter α and β is expected to improve the convergence to $\mathrm{O}(h^{k+3/2})$ according to [3]. We come back to these effects in Section 4 on numerical experiments and stress that, at least in the a posteriori error analysis, the constants α and β shall be monitored as well as t and h.

3. A posteriori error bound and adaptive algorithm

For the regular triangulation $\mathscr{T}$ of Ω in (closed) triangles or parallelograms let $\mathscr{K}$ be the (finite) set of all nodes and let $\mathscr{N}:=\mathscr{K}\cap\Omega$ be the set of interior nodes. We assume that the triangulation matches the domain exactly, i.e., $\cup\mathscr{T}=\overline{\Omega}$ and two distinct elements T_1 and T_2 in $\mathscr{T}$ are either disjoint, or $T_1\cap T_2$ is a complete edge or a common vertex of both, T_1 and T_2 (there are no hanging nodes). The set of edges $E=\mathrm{conv}\{x,y\}$ for two distinct $x,y\in\mathscr{N}$ is denoted as $\mathscr{E}$. Their union $\cup\mathscr{E}$ is the skeleton of all element boundaries, i.e., the set of all points in $\overline{\Omega}$ which belong to some edge. With each edge, we associate a unit normal vector n_E which coincides with the exterior normal if the edge E belongs to the boundary $\partial\Omega$. For a $\mathscr{T}$-piecewise uniformly continuous function, the square brackets $[\cdot]$ are defined as the jump over the edges: if $E=T_+\cap T_-$ is a common edge of two distinct T_+ and T_- in $\mathscr{T}$ then, for $x\in E$, the jump $[G](x)$ is the limit of $G(x+\epsilon n_E)-G(x-\epsilon n_E)$ as $\epsilon\to 0^+$. (The limit exists if $x\notin\mathscr{K}$ since $x\pm\epsilon n_E\in T_\pm$ and G is uniformly continuous on each $T_\pm$.) In this way, $[G]$ is defined on the skeleton $\cup\mathscr{E}\setminus\partial\Omega$ of all inner boundaries of elements. Its definition on the boundary has to be specified separately with special values g as exterior values: $[G](x):=g(x)-G|_{\partial\Omega}(x)$ for $x\in\partial\Omega\setminus\mathscr{N}$.

In the following the diameter of T is denoted as h_T and the length of E is h_E, where h is a characteristic (global) mesh-size. The triangulation satisfies the minimum angle condition, i.e., the angles in the triangles or parallelograms are assumed to belong to the interval $(c_\theta,\pi-c_\theta)$ for some positive constant c_θ and so are bounded uniformly away from 0 and π.

The discrete problem is supposed to generate discrete solutions $(\vartheta_h,w_h,\gamma_h)\in H_0^1(\Omega)^2\times H_0^1(\Omega)\times L^2(\Omega)$ which are neither expected to be uniquely determined nor to belong to a discrete space $V_h\times W_h\times\Gamma_h$. We merely suppose that $(\vartheta_h,w_h,\gamma_h)$ is $\mathscr{T}$-piecewise smooth (such that all the derivatives in (3.1) and related traces and jumps on the edges exist in the classical sense and are integrable). As a minimal condition, we suppose $(\vartheta_h,w_h,\gamma_h)$ satisfies (2.11) and (2.12) for all $(\phi_h,v_h,\eta_h)\in\mathscr{S}_1(\mathscr{T})^2\times\mathscr{S}_1(\mathscr{T})\times\mathscr{P}_0(\mathscr{T})$. For each element $T\in\mathscr{T}$, we define our error indicator η_T by

$$\begin{aligned}\eta_T^2:=\int_T\Big(&h_T^2|f-\mathrm{div}(\gamma_h+\alpha(\vartheta_h-\nabla w_h))|^2+h_T^2|\gamma_h+\alpha(\vartheta_h-\nabla w_h)-\mathrm{div}\,\mathbb{C}\varepsilon(\vartheta_h)|^2+|\mathrm{rot}\,\rho_1|^2\\&+|\rho_1|^2+t^{-2}|\rho_2|^2\Big)\,\mathrm{d}x+\sum_{E\in\mathscr{E},\,E\subset\partial T}h_E\int_E\Big(|[\gamma_h+\alpha(\vartheta_h-\nabla w_h)]\cdot n_E|^2+|[\mathbb{C}\varepsilon(\vartheta_h)]\cdot n_E|^2\Big)\,\mathrm{d}s.\end{aligned}\tag{3.1}$$

Here, $\rho_1\in H_0(\mathrm{rot};\Omega)$ and $\rho_2\in L^2(\Omega)$ is an arbitrary (global) split of the shear-residual

$$\rho_1+\rho_2=\rho:=t^2\gamma_h-(1-\alpha t^2)(\vartheta_h-\nabla w_h).\tag{3.2}$$

Let $(\vartheta,w,\gamma)\in H_0^1(\Omega)^2\times H_0^1(\Omega)\times L^2(\Omega)$ denote the exact solution to (2.4) and (2.5). With an (h,t,α)-independent constant c_1, we then have the a posteriori error estimate

$$\|(\vartheta-\vartheta_h,w-w_h)\|_{H_0^1(\Omega)}^2+\|\gamma-\gamma_h+\alpha(\vartheta-\vartheta_h-\nabla(w-w_h))\|_{H^{-1}(\mathrm{div})\cap t\cdot L^2}^2\leqslant c_1\min_{\varrho=\varrho_1+\varrho_2}\sum_{T\in\mathscr{T}}\eta_T^2.\tag{3.3}$$

Remark 1.

(i) The main advantage of (and motivation for) the formulation (3.1) is that (3.3) holds uniformly in t and α.
(ii) Verfürth's inverse estimate technique [17] (with Theorem 2 below) shows that the estimate (3.3) is sharp: up to higher order terms, the converse inequality holds (for some terms even in a more local form).
(iii) The point is that the optimal global additive split $\rho = \rho_1 + \rho_2$ is not directly computable and it remains open whether the upper bound suggested below is efficient. Indeed, factors such as h_T/t might be very large and so could result in a huge overestimation.

Example 1. If $\rho_2 = \rho$ we obtain (with a Poincaré inequality on T [14]) in (3.1) that

$$\int_T (|\operatorname{rot}\rho_1|^2 + |\rho_1|^2 + t^{-2}|\rho_2|^2)\,\mathrm{d}x \leqslant h_T^2 t^{-2}/\pi \int_T (1-\alpha t^2)|\nabla\vartheta_h - D^2 w_h|^2)\,\mathrm{d}x \tag{3.4}$$

($D^2 w_h$ denotes the 2×2-matrix of all second-order partial derivatives).

Example 2. If α is constant on Ω and $\eta_h = t^2\gamma_h$ we may choose $\rho_1 = (1-\alpha t^2)(\vartheta_h - \nabla w_h)$ and obtain in (3.1) that

$$\int_T (|\operatorname{rot}\rho_1|^2 + |\rho_1|^2 + t^{-2}|\rho_2|^2)\,\mathrm{d}x \leqslant (1-\alpha t^2)\int_T (|\operatorname{rot}\vartheta_h|^2 + |\vartheta_h - \nabla w_h|^2)\,\mathrm{d}x + \int_T |\gamma_h|^2\,\mathrm{d}x. \tag{3.5}$$

Example 3. Below we employ the estimate from Theorem 6 of Section 5 from which we obtain

$$\int_T (|\operatorname{rot}\rho_1|^2 + |\rho_1|^2 + t^{-2}|\rho_2|^2)\,\mathrm{d}x \leqslant c_8 h_T/t \int_T |\nabla\vartheta_h - D^2 w_h|^2\,\mathrm{d}x. \tag{3.6}$$

Other decompositions are possible involving continuous or discrete Helmholtz decompositions. The disadvantage of (3.1) then is that any such decomposition is global and so a numerical realization may be expensive.

Since it involves the smallest factor h_T/t amongst all above mentioned splits which are applicable for $\mathscr{T}$-piecewise constant α, we employ in the numerical examples below estimator (1.4) with computable local contributions from Example 3, namely

$$\begin{aligned}\eta_T^2 := \int_T \Big(& h_T^2 |f - \operatorname{div}(\gamma_h + \alpha(\vartheta_h - \nabla w_h))|^2 + h_T^2 |\gamma_h + \alpha(\vartheta_h - \nabla w_h) - \operatorname{div}\mathbb{C}\varepsilon(\vartheta_h)|^2 \\ & + h_T/t\,|\nabla\vartheta_h - D^2 w_h|^2\Big)\,\mathrm{d}x + \sum_{E\in\mathscr{E},E\subset\partial T} h_E \int_E \Big(|[\gamma_h + \alpha(\vartheta_h - \nabla w_h)]\cdot n_E|^2 + |[\mathbb{C}\varepsilon(\vartheta_h)]\cdot n_E|^2\Big)\,\mathrm{d}s.\end{aligned} \tag{3.7}$$

Theorem 1. *The error indicators* (3.7) *satisfy* (3.3) *with an* (h,t,α)*-independent constant* c_1 *that depends only on* Ω *and the constant* c_ϑ *in the minimum angle condition.*

The proof of Theorem 1 will be given in Section 5. It motivates the usage of the error indicators (3.7) for adaptive mesh-refining.

Adaptive Algorithm (A).

(a) Start with coarse mesh $\mathscr{T}_0$.
(b) Solve discrete problem with respect to $\mathscr{T}_k$ with N degrees of freedom.
(c) Compute η_T for all $T\in\mathscr{T}_k$.
(d) Compute error bound $\eta_N := \left(\sum_{T\in\mathscr{T}_k}\eta_T^2\right)^{1/2}$ and terminate or go to (e).
(e) Mark element T red iff $\eta_T \geqslant \frac{1}{2}\max_{T'\in\mathscr{T}_k}\eta_{T'}$.
(f) Refine marked elements, update mesh $\mathscr{T}_k$ and go to (b).

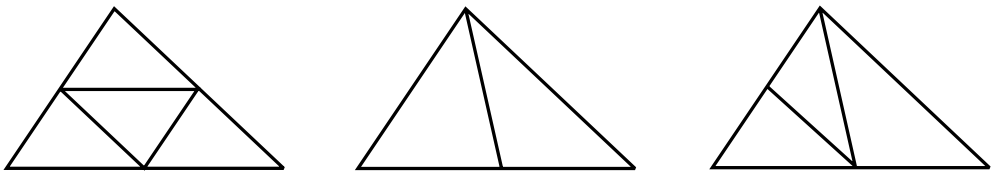

Fig. 1. Red–green–blue refinement of a triangle.

We employ here red–green–blue refining procedures (cf. Fig. 1). Red-refining means to bisect the sides of one marked triangle and remesh with four congruent triangles. The neighboring, not marked elements are split in a way, that ever one longest side is divided. For this purpose one triangle is to cut into halves (green refining) or we have to split the triangle into three triangles (blue refining). This way we avoid hanging nodes as well as degenerated elements.

4. Numerical experiments

4.1. Comparison with Kirchhoff solution

Since the solutions of (1.1) and (1.2) tend to the solution of the Kirchhoff equation when $t \to 0$, we first compare our estimator with the exact value of (1.3) for the (different) solution

$$w(x,y) = (x^2 - 1/4)^2 (y^2 - 1/4)^2 \quad \text{with} \quad (w, \vartheta := \nabla w) \in H_0^1(\Omega) \times H_0^1(\Omega)^2. \tag{4.1}$$

The plate $(x,y) \in \Omega := (-1/2, +1/2)^2$ with thickness $t = 0.001$ has material parameters $E = 10.92$, $v = 0.3$ and is loaded with $f = Ekt^3/(12(1-v^2))\Delta\Delta w$. Owing to the symmetry we compute only one quarter $[0, 0.5]^2$ with an initial mesh $\mathscr{T}_0$ of $N = 52$ degrees of freedom, cf. Fig. 2.

Numerical studies confirmed that the discrete problem (2.11) and (2.12) is asymptotically stable against the parameters α and β but preasymptotic performance as well as convergence rates strongly depend on it (cf. [18]). Summarizing our experience we prosecute here two strategies for a choice of parameters in (2.4). First, we choose model dependent but fixed parameters α and β. Using a characteristic size of plate domain $l := l(\Omega)$ and plate thickness t, $l \gg t$, we employ

$$\alpha = \frac{1}{lt} \quad \text{and} \quad \beta = \frac{t^2}{1 - \alpha t^2}. \tag{4.2}$$

Secondly, we adapt α to the finite element mesh-size with $\alpha = \mathrm{O}(h^{-2})$ (cf. [11,18]), computing element-wise

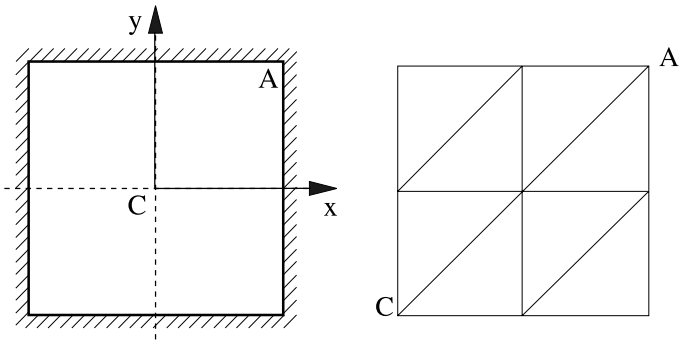

Fig. 2. Example of Section 4.1.

$$\alpha = \alpha(T) = \frac{1}{h_T^2 + t^2} \tag{4.3}$$

and β as in (4.2). Both numerical rules imply $0 < \alpha < t^2$ and avoid spurious modes on coarse meshes. In the examples of this paper we set $l = 1$ in (4.2).

To measure the solution error we compute the H^1-norm of the difference between the Kirchhoff and the finite element solution for the displacement as well as for the rotation vector.

$$e(w, \vartheta) := \left(\|w - w_h\|^2_{H^1_0(\Omega)} + \|\vartheta - \vartheta_h\|^2_{H^1_0(\Omega)} \right)^{1/2}. \tag{4.4}$$

For evaluating (1.3) resp. (3.3) we add to (4.4) the normed difference of scaled shear stress vectors $\gamma - \gamma_h$ whereby the shear stress in the Kirchhoff theory is introduced by additional equilibrium conditions [16]. The norm (2.7) is not computable and so estimated owing to duality arguments and a Poincaré inequality

$$\|q\|_{H^{-1}(\Omega)} \leqslant c_3 \|hq\|_{L^2(\Omega)} \tag{4.5}$$

for $\mathscr{T}$-piecewise polynomials q with elementwise vanishing integral mean. The estimate (4.5) is applicable here because the finite element solution and, as an exception, the analytical solution is a $\mathscr{T}$-piecewise polynomial. Ignoring the (h-independent) constant c_3, we approximate (1.3) by

$$\begin{aligned} e(w, \vartheta, \gamma) := \Big(& e(w, \vartheta)^2 + (h_T^2 + t^2) \|\gamma - \gamma_h + \alpha(\vartheta - \vartheta_h - \nabla(w - w_h))\|^2_{L^2(\Omega)} \\ & + h_T^2 \|\operatorname{div}(\gamma - \gamma_h + \alpha(\vartheta - \vartheta_h - \nabla(w - w_h)))\|^2_{L^2(\Omega)} \Big)^{1/2}. \end{aligned} \tag{4.6}$$

For comparison we also calculated the natural energy error

$$e_h := \left(\|\mathbb{C}^{1/2} \varepsilon(\vartheta - \vartheta_h)\|^2 + t^{-2} \|\vartheta - \vartheta_h - \nabla(w - w_h)\|^2 \right)^{1/2}. \tag{4.7}$$

Fig. 3 displays the error results for uniformly refined meshes and for parameters α resp. β being (a) constant (4.2) and (b) mesh-adapted (4.3). Here and below the error terms are plotted vs the number of degrees of freedom N in a log / log-scale $\eta_N := \eta_{\mathscr{T}}$; owing to $N \propto h^{-2}$ in two dimensions, a slope $-1/2$ in the figures corresponds to an experimental convergence rate 1. The estimate η_N appears to be very accurate in case (a) as well as in case (b), where the error norm of (3.3) shows a poor convergence behavior (the estimate is accurate, the error is poor).

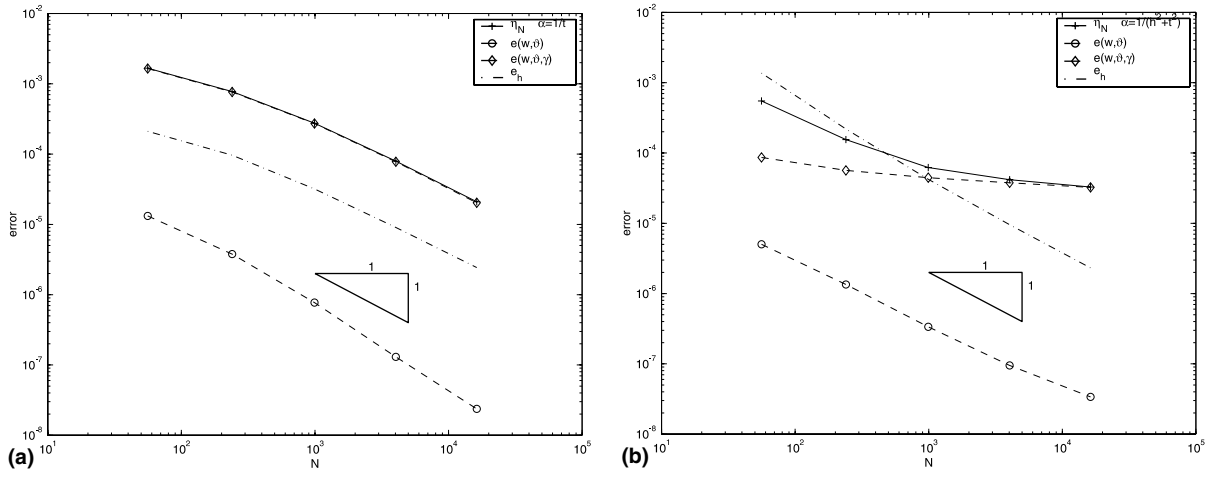

Fig. 3. Exact solution error (1.3) and error estimator (3.7) for uniform mesh refinements: (a) $\alpha = 1/t$; (b) $\alpha = 1/(h_T^2 + t^2)$.

The error contributions of displacement and rotations (4.4) converges quadratically (in both cases). Hence the shear-error term dominates but is estimated well. Our explanation for the poor convergence behavior in case (b) is that the proper mesh-depending choice of α and β is not well-balanced with our strong norm of the physical shear-error. This is underlined by our observation that the energy error (4.7) converges quadratically in both cases.

4.2. Numerical examples for practical error computation

In the first example an L-shaped plate $(-1,1)^2 \setminus [0,1]^2$ is clamped along the two edges of the domain which form the re-entering corner and is free at the remaining boundary. The (unknown) exact solution is expected to be singular near the origin at the re-entering corner even though the load is uniformly distributed, $f = 1$. The material parameters are constant as in Section 4.1.

We monitor now the error estimation with different plate thickness $t = 0.1, 0.01$, and 0.001. Again we apply schemes (4.2) and (4.3) for the parameters α and β. We start our finite element computation with a coarse mesh $\mathcal{T}_0$ with 107 degrees of freedom (Fig. 4(a)) and refine uniformly but presumably sub-optimal. The convergence rate of error estimator $\eta_{\mathcal{T}}$ with (3.7) is smaller than one (Fig. 5, dashed lines). To assess

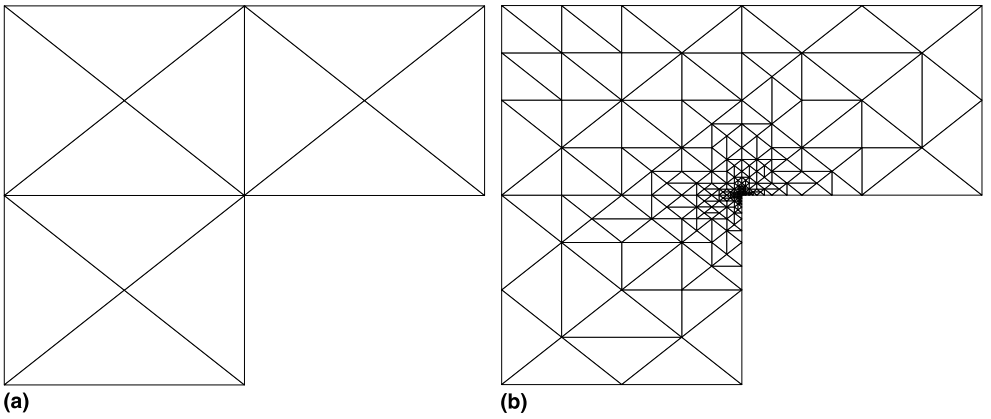

Fig. 4. Finite element meshes in Example of Section 4.2: (a) initial mesh $\mathcal{T}_0$; (b) adaptive refined mesh $\mathcal{T}_7$.

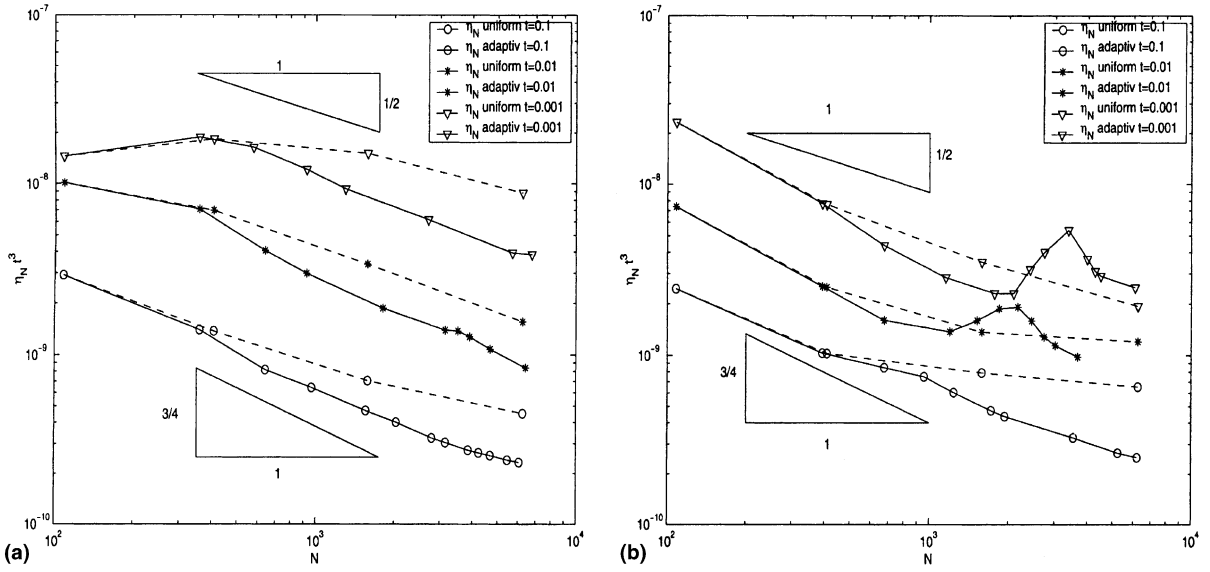

Fig. 5. Error estimation (3.7) for uniform and adaptive mesh refinements: (a) $\alpha = 1/t$; (b) $\alpha = 1/(h_T^2 + t^2)$.

the quality of error estimation for a non-uniform mesh, we employed the adaptive mesh-refining Algorithm (A) of Section 3. A typical mesh $\mathscr{T}_7$ after seven adaptive refinement steps is shown in Fig. 4 (here for: $t = 0.01$ with (4.3)). The computations show the expected superiority of adaptive refinement techniques, but also we observe a poor convergence rate of η_N if α and β are mesh-adapted.

The error in the energy norm (4.7) is monitored as well. From [9] we know, that (4.7) equals the square root of

$$C - \|\mathbb{C}^{1/2}\varepsilon(\vartheta_h)\|^2 + t^{-2}\|\nabla w_h - \vartheta_h\|^2 - 2\big((t^{-2} - \alpha)(\nabla w_h - \vartheta_h) - \gamma_h; \nabla w_h - \vartheta_h\big) \tag{4.8}$$

with the real number

$$C := (f; w) = \|\mathbb{C}^{1/2}\varepsilon(\vartheta)\|^2 + t^{-2}\|\vartheta - \nabla w\|^2.$$

An extrapolation technique yields $C = 0.8366 \times 10^{-13}$ if $t = 0.1$ and $C = 0.787 \times 10^{-19}/t^6$ else (cf. [9] for details). Fig. 6 displays the convergence rates for the relative energy error $e_N := e_h/\sqrt{C}$ with uniform mesh refinement (dashed lines) which is less than 1 if α is constant and $3/2$ in case of mesh-adapted α. With adaptive refining algorithms we obtain a significant reduction of error e_N up to convergence rate 2 in both cases.

Finally, we consider the rectangular steel plate of Fig. 7 loaded by two stamps of 0.1 m × 0.1 m (e.g., caused by fork-lift trucks) with $f = 10^6$ N/m (f vanishes outside of that region), $E = 2.1 \times 10^{12}$ N/m^2, $v = 0.3$, $t = 0.1$ m. On the three marked sides the plate is simply supported by hard support. (Hard support

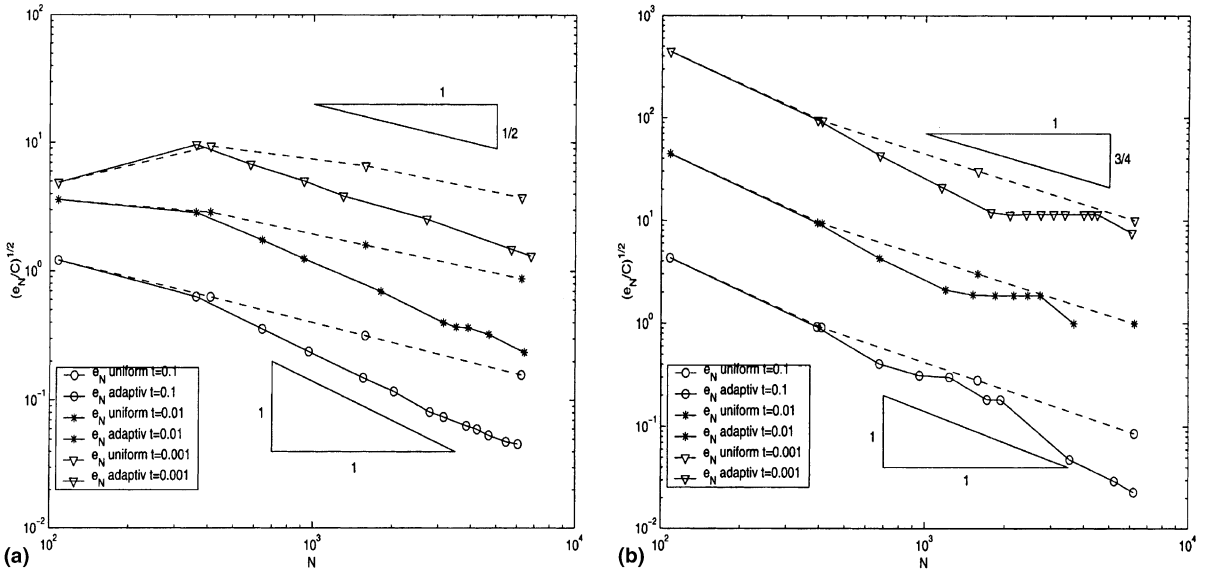

Fig. 6. Energy error (4.8) for uniform and adaptive mesh refinements: (a) $\alpha = 1/t$; (b) $\alpha = 1/(h_T^2 + t^2)$.

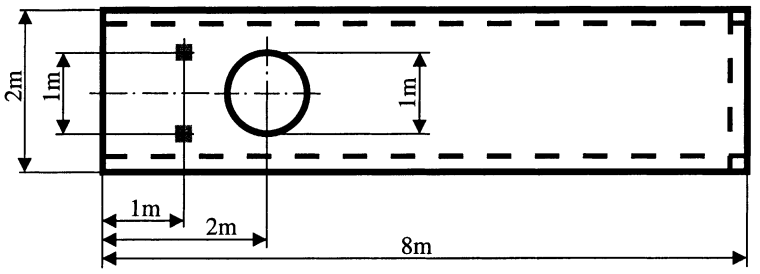

Fig. 7. Sheet metal.

means that not only the displacements but also the tangential component of the rotation is forced to zero.) Owing to the symmetry we compute one half of the domain. The coarse initial mesh consists of 17 finite elements with $N = 126$ degrees of freedom. Fig. 8 displays the meshes generated by the Adaptive Algorithm (A). Since load function f is evaluated at the Gauss points within T, f is reflected correctly only for meshes which are sufficiently fine around the load. If the mesh-size is small compared to stamp load (or at least decreased to a comparable size) the load singularity should be of minor influence.

The error estimator η_N is plotted in Fig. 9 vs the number of degrees of freedom N and compared with uniform refinement technique. The vanishing influence of load singularity is seen here by a high error-

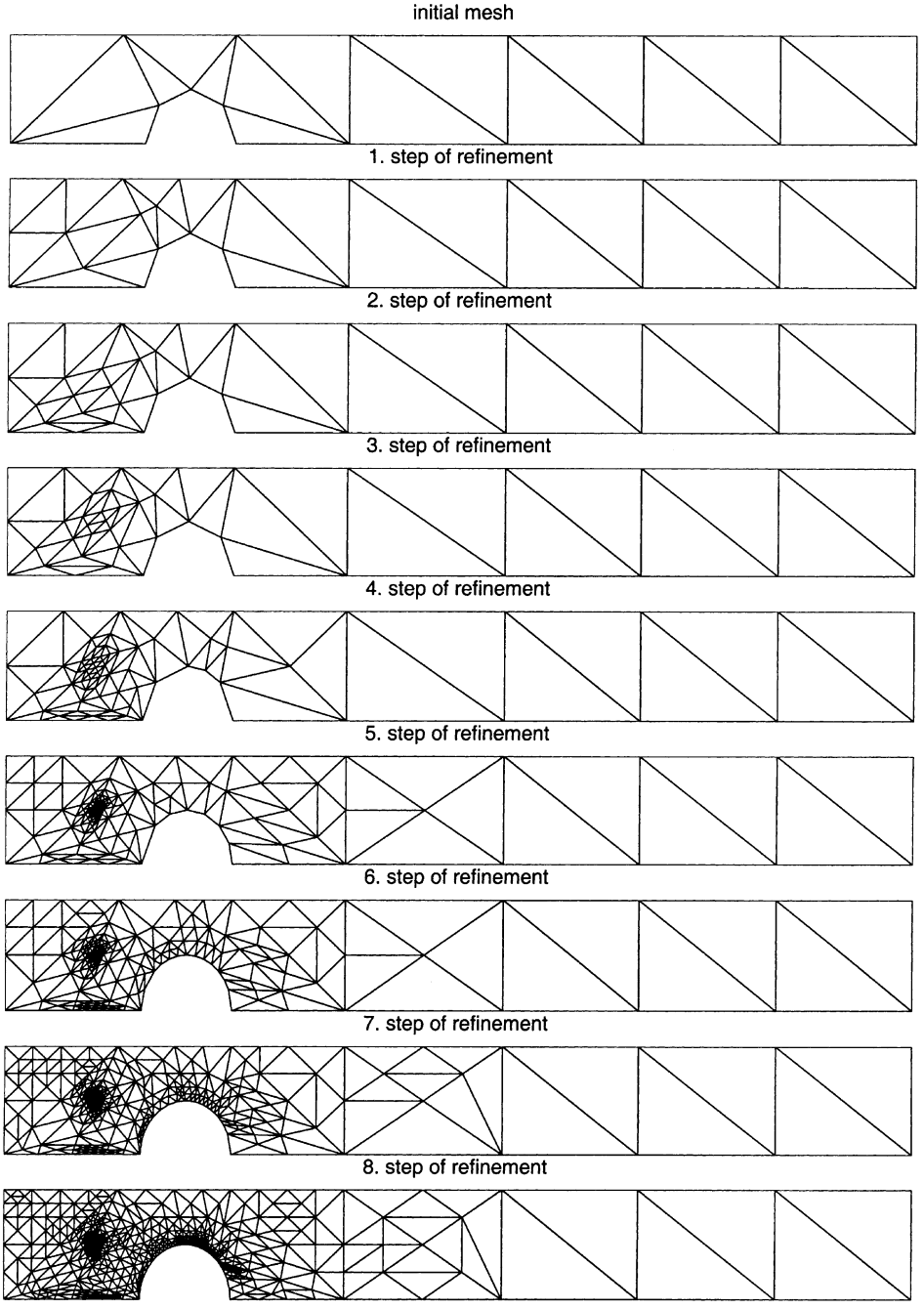

Fig. 8. Adaptive refined meshes.

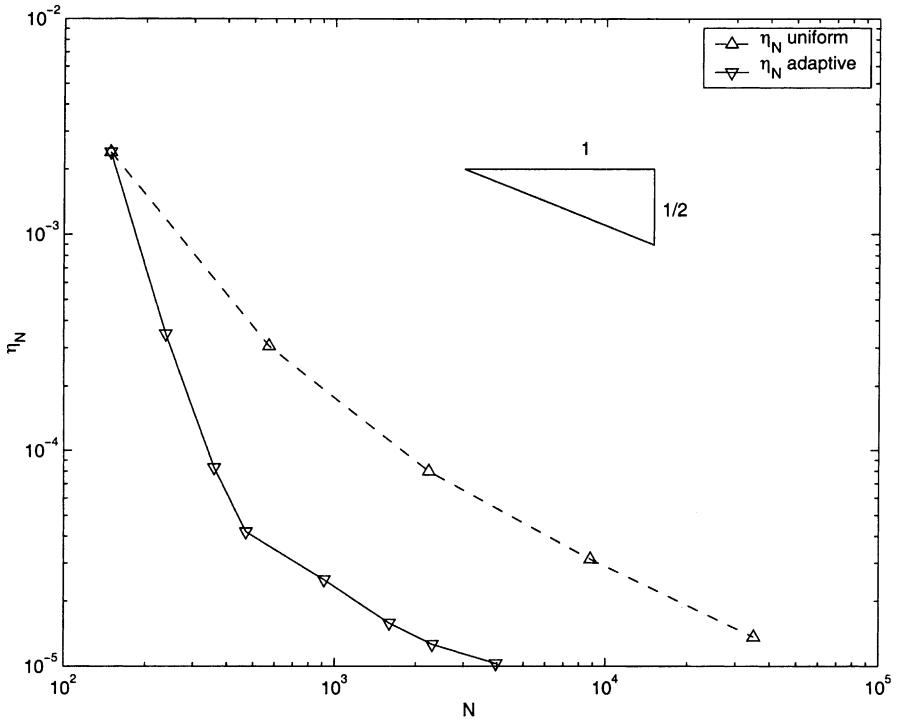

Fig. 9. Error estimation (3.7) for sheet metal.

reduction in the beginning of the adaptive mesh-refining and the asymptotic convergence rate 1 for finer meshes. Although the improvement of Algorithm (A) over a uniform mesh-refinement is possibly not well displayed by the considered error-norm (and so by η_N, we apply (4.3) only) it can be deduced from Fig. 9 that the adaptive algorithm reduces the computational effort significantly.

5. Proof of reliability

Throughout this section, we suppose $(\vartheta, w, \gamma) \in H_0^1(\Omega)^2 \times H_0^1(\Omega) \times L^2(\Omega)$ solves (2.4) and (2.5) and $(\vartheta_h, w_h, \gamma_h)$ solves (2.11) and (2.12) at least for all $(\phi_h, v_h, \eta_h) \in \mathscr{S}_1(\mathscr{T})^2 \times \mathscr{S}_1(\mathscr{T}) \times \mathscr{P}_0(\mathscr{T})$.

For compact notation, let $h_{\mathscr{T}} \in L^\infty(\Omega)$ and $h_{\mathscr{E}} \in L^\infty(\cup\mathscr{E})$ be given as $\mathscr{T}$- resp. $\mathscr{E}$-piecewise constant weights

$$h_{\mathscr{T}}|_T := h_T \quad \text{and} \quad h_{\mathscr{E}}|_E := h_E \quad (T \in \mathscr{T}; E \in \mathscr{E}). \tag{5.1}$$

Set

$$\phi := \vartheta - \vartheta_h \in H_0^1(\Omega)^2, \quad \omega := w - w_h \in H_0^1(\Omega), \quad \zeta := \gamma_h - \gamma - \alpha(\phi - \nabla\omega) \in L^2(\Omega)^2$$

and define the linear functionals $F : H_0^1(\Omega)^2 \to \mathbb{R}$, $G : H_0^1(\Omega) \to \mathbb{R}$, and $J : L^2(\Omega)^2 \to \mathbb{R}$ by

$$F(\varphi) := \int_\Omega \varepsilon(\phi) : \mathbb{C}\varepsilon(\varphi)\,\mathrm{d}x - \int_\Omega \zeta \cdot \varphi\,\mathrm{d}x,$$

$$G(v) := \int_\Omega \zeta \cdot \nabla v\,\mathrm{d}x,$$

$$J(\eta) := -\int_\Omega (t^2\zeta + \phi - \nabla\omega) \cdot \eta\,\mathrm{d}x,$$

for all

$$(\varphi, v, \eta) \in X_t := H_0^1(\Omega)^2 \times H_0^1(\Omega) \times (H^{-1}(\mathrm{div}; \Omega) \cap t \cdot L^2(\Omega)),$$

cf. (2.9) for the norm in the last factor.

Theorem 2 (Arnold et al. [2]). *There exists positive constants c_4 and c_5 which are independent of $(t, \phi, \omega, \zeta, F, G, J)$ such that*

$$c_4 \|(F, G, J)\|_{X_t^*} \leqslant \|(\phi, \omega, \zeta)\|_{X_t} \leqslant c_5 \|(F, G, J)\|_{X_t^*}. \tag{5.2}$$

Theorem 2 yields an estimate of $\|(\phi, \omega, \zeta)\|_{X_t}$ so that it suffices for the proof of (3.3) to prove separate estimates for $\|F\|_{H^{-1}(\Omega)}$, $\|G\|_{H^{-1}(\Omega)}$, and $\|J\|_{(H^{-1}(\mathrm{div}) \cap t \cdot L^2)^*}$.

The bounds for $\|F\|_{H^{-1}(\Omega)}$ and $\|G\|_{H^{-1}(\Omega)}$ are standard [17] and can be proved with integration by parts and the subsequent technical result on the approximation and stability properties of the Clement approximation operator [10,17]. Let $h_{\mathscr{T}}$ denote the mesh-sizes and $h_{\mathscr{E}}$ denote the edge-sizes on Ω and $\cup\mathscr{E}$ with respect to $\mathscr{T}$.

Theorem 3 (Clément [10]). *There exists a positive constant c_6 that depends on c_θ from the minimal angle-condition and the aspect ratio of elements in $\mathscr{T}$ and such that, given any $(\varphi, v) \in H_0^1(\Omega)^3$, there exists some $(\varphi_h, v_h) \in \mathscr{S}^1(\mathscr{T})^3$ with*

$$\begin{aligned} &\|h_{\mathscr{T}}^{-1}(\varphi - \varphi_h, v - v_h)\|_{L^2(\Omega)} + \|h_{\mathscr{E}}^{-1/2}(\varphi - \varphi_h, v - v_h)\|_{L^2(\cup\mathscr{E})} + \|(D\varphi_h, \nabla v_h)\|_{L^2(\Omega)} \\ &\quad \leqslant c_6 \|(D\varphi, \nabla v)\|_{L^2(\Omega)} \leqslant c_6 \|(\varphi, v)\|_{H^1(\Omega)}. \end{aligned} \tag{5.3}$$

The bounds for $\|F\|_{H^{-1}(\Omega)}$ and $\|G\|_{H^{-1}(\Omega)}$ are shown simultaneously.

Theorem 4. *We have*

$$\begin{aligned} \|(F, G)\|_{H^{-1}(\Omega)} \leqslant c_6 \Big(&\|h_{\mathscr{E}}^{1/2}[(\mathbb{C}\varepsilon(\vartheta_h), \gamma_h + \alpha(\vartheta_h - \nabla w_h))] n_{\mathscr{E}}\|_{L^2(\cup\mathscr{E})} \\ &+ \|h_{\mathscr{T}}(\mathrm{div}_{\mathscr{T}} \mathbb{C}\varepsilon(\vartheta_h) - \gamma_h - \alpha(\vartheta_h - \nabla w_h), f - \mathrm{div}_{\mathscr{T}}(\gamma_h + \alpha(\vartheta_h - \nabla w_h)))\|_{L^2(\Omega)} \Big). \end{aligned} \tag{5.4}$$

Proof. Direct calculations with (2.1)–(2.3), (2.11) show for all $(\varphi, v) \in H_0^1(\Omega)^3$ with $(\varphi_h, v_h) \in \mathscr{S}^1(\mathscr{T})^3$ as in Theorem 3 that

$$\begin{aligned} F(\varphi) + G(v) &= a(\phi, \omega; \varphi, v) + b(\varphi, v; \gamma - \gamma_h) \\ &= a(\phi, \omega; \varphi - \varphi_h, v - v_h) + b(\varphi - \varphi_h, v - v_h; \gamma - \gamma_h) \\ &= \int_\Omega f(v - v_h)\,\mathrm{d}x - a(\phi, \omega; \varphi_h, v_h) - b(\varphi_h, v_h; \gamma - \gamma_h). \end{aligned} \tag{5.5}$$

Let $\mathrm{div}_{\mathscr{T}}$ denote the $\mathscr{T}$-piecewise action of the divergence operator. The $\mathscr{T}$-piecewise integration by parts with a detailed inspection of the two contributions on each interior edge $E = \partial T_- \cap \partial T_+$ from the two neighboring elements $T_\pm$ show in (5.5) that

$$\begin{aligned} F(\varphi) + G(v) &= \int_\Omega f(v - v_h)\,\mathrm{d}x - \int_\Omega \mathbb{C}\varepsilon(\vartheta_h) : D(\varphi - \varphi_h)\,\mathrm{d}x - \int_\Omega (\gamma_h + \alpha(\vartheta_h - \nabla w_h)) \cdot (\varphi - \varphi_h - \nabla(v - v_h))\,\mathrm{d}x \\ &= \int_\Omega (\mathrm{div}_{\mathscr{T}} \mathbb{C}\varepsilon(\vartheta_h) - \gamma_h - \alpha(\vartheta_h - \nabla w_h)) \cdot (\varphi - \varphi_h)\,\mathrm{d}x - \int_{\cup\mathscr{E}} [\mathbb{C}\varepsilon(\vartheta_h)] n_{\mathscr{E}} \cdot (\varphi - \varphi_h)\,\mathrm{d}s \\ &\quad - \int_\Omega (f - \mathrm{div}_{\mathscr{T}}(\gamma_h + \alpha(\vartheta_h - \nabla w_h))) \cdot (v - v_h)\,\mathrm{d}x + \int_{\cup\mathscr{E}} [\gamma_h + \alpha(\vartheta_h - \nabla w_h)] \cdot n_{\mathscr{E}} (v - v_h)\,\mathrm{d}s. \end{aligned} \tag{5.6}$$

Cauchy inequalities show in (5.6) that

$$\begin{aligned} F(\varphi)+G(v) \leqslant & + \|h_{\mathscr{E}}^{1/2}[\mathbb{C}\varepsilon(\vartheta_h)]n_{\mathscr{E}}\|_{L^2(\cup\mathscr{E})}\|h_{\mathscr{E}}^{-1/2}(\varphi-\varphi_h)\|_{L^2(\cup\mathscr{E})} \\ & \times \|h_{\mathscr{T}}(\mathrm{div}_{\mathscr{T}}\mathbb{C}\varepsilon(\vartheta_h)-\gamma_h-\alpha(\vartheta_h-\nabla w_h))\|_{L^2(\Omega)}\|h_{\mathscr{T}}^{-1}(\varphi-\varphi_h)\|_{L^2(\Omega)} \\ & + \|h_{\mathscr{T}}(f-\mathrm{div}_{\mathscr{T}}(\gamma_h+\alpha(\vartheta_h-\nabla w_h)))\|_{L^2(\Omega)}\|h_{\mathscr{T}}^{-1}(v-v_h)\|_{L^2(\Omega)} \\ & + \|h_{\mathscr{E}}^{1/2}[\gamma_h+\alpha(\vartheta_h-\nabla w_h)]\cdot n_{\mathscr{E}}\|_{L^2(\cup\mathscr{E})}\|h_{\mathscr{E}}^{-1/2}(v-v_h)\|_{L^2(\cup\mathscr{E})} \end{aligned}$$

and then Theorem 3 yields

$$\begin{aligned} (F(\varphi)+G(v))/(c_6\|(\varphi,v)\|_{H^1(\Omega)}) \leqslant & \|h_{\mathscr{E}}^{1/2}[\mathbb{C}\varepsilon(\vartheta_h)]n_{\mathscr{E}}\|_{L^2(\cup\mathscr{E})}+\|h_{\mathscr{E}}^{1/2}[\gamma_h+\alpha(\vartheta_h-\nabla w_h)]n_{\mathscr{E}}\|_{L^2(\cup\mathscr{E})} \\ & + \|h_{\mathscr{T}}(\mathrm{div}_{\mathscr{T}}\mathbb{C}\varepsilon(\vartheta_h)-\gamma_h-\alpha(\vartheta_h-\nabla w_h))\|_{L^2(\Omega)} \\ & + \|h_{\mathscr{T}}(f-\mathrm{div}_{\mathscr{T}}(\gamma_h+\alpha(\vartheta_h-\nabla w_h)))\|_{L^2(\Omega)}. \qquad \square \end{aligned}$$

Proof of Inequality (3.3). The combination of Theorems 2 and 4 shows the assertion. □

To derive a local estimate of $\|J\|_{(H^{-1}(\mathrm{div})\cap t\cdot L^2)^*}=\|\rho\|_{H_0(\mathrm{rot})+t^{-1}\cdot L^2}$, we employ the following estimate based on a deeper result in interpolation theory due to Tartar [15].

Theorem 5 (Brenner and Scott [7]). *For each $T\in\mathscr{T}$ and $v\in H^1(T)$ we have*

$$\inf_{v=v_0+v_1}\left(\|v_0\|_{L^2(T)}^2+t^2\|\nabla v_1\|_{L^2(T)}^2\right)\leqslant c_7 t\|v\|_{L^2(T)}\left(\|\nabla v\|_{L^2(T)}+h_T^{-1}\|v\|_{L^2(T)}\right), \tag{5.7}$$

where $v_0\in L^2(T)$ and $v_1\in H_0^1(T)$ is an arbitrary additive split of v. The constant c_7 depends on the shape but not on the size of T and does neither depend on v nor on (t,h_T).

Proof. The combination of Propositions 1, 2, 3 in [7] show that the left-hand side of (5.7) is bounded by $2\sqrt{t}\|v\|_{X(\infty,T)}$ while the right-hand side of (5.7) is an upper bound of this term (cf. [7] and especially (3.20) therein for notation and proofs). □

In case that α and γ_h are constant on each element T in $\mathscr{T}$, we deduce an explicit upper bound of the global norm $\|J\|_{(H^{-1}(\mathrm{div})\cap t\cdot L^2)^*}$ of the residual J. Note that this upper bound is local in the sense that it consists of a sum of local contributions.

Theorem 6. *We have (D^2w_h denotes the 2×2-matrix of all second-order partial derivatives)*

$$\|J\|_{(H^{-1}(\mathrm{div})\cap t\cdot L^2)^*}\leqslant c_8\left(\sum_{T\in\mathscr{T}}h_T/t\int_T|\nabla\vartheta_h-D^2w_h|^2\,\mathrm{d}x\right)^{1/2}. \tag{5.8}$$

The constant c_8 depends on the shape but not on the size of the elements and does neither depend on ρ nor on (t,h_T).

Proof. The choice of $v:=\rho|_T$ in Theorem 5 reveals existence of $v_2|_T\in L^2(T)$ and $v_1|_T\in H_0^1(T)$ with

$$t^{-2}\|v_0\|_{L^2(T)}^2+\|\nabla v_1\|_{L^2(T)}^2\leqslant c_7 t^{-1}\|v\|_{L^2(T)}\left(\|\nabla v\|_{L^2(T)}+h_T^{-1}\|v\|_{L^2(T)}\right) \tag{5.9}$$

on each element $T\in\mathscr{T}$. Recall that the integral mean on T of ρ vanishes and so a Poincaré inequality gives $\|v\|_{L^2(T)}\leqslant h_T/\pi\|\nabla v\|_{L^2(T)}$ [14]. Utilizing this in (5.9) leads to

$$t^{-2}\|v_0\|_{L^2(T)}^2+\|\nabla v_1\|_{L^2(T)}^2\leqslant c_7 h_T t^{-1}(1+1/\pi)\|\nabla v\|_{L^2(T)}^2. \tag{5.10}$$

The composition of $v_j|_T$ for all $T \in \mathscr{T}$, i.e., the functions $\rho_j \in L^2(\Omega)$ with $\rho_j|_T := v_j|_T$, $j = 0, 1$, satisfy $\rho = \rho_0 + \rho_1$ and, owing to $v_1 = 0$ on ∂T for each $T \in \mathscr{T}$, $\rho_1 \in H_0^1(\Omega) \subset H_0(\mathrm{rot}; \Omega)$. Since the additive split $\rho = \rho_0 + \rho_1$ (with $\rho_2 := \rho_0$) is possible in the norm in (2.10) we have

$$\|\rho\|^2_{H_0(\mathrm{rot})+t^{-1}\cdot L^2} \leqslant \|\rho_1\|^2_{H_0(\mathrm{rot};\Omega)^2} + t^{-2}\|\rho_0\|^2_{L^2(\Omega)}. \tag{5.11}$$

Since v_1 vanishes on ∂T, $T \in \mathscr{T}$, Friedrich's inequality gives $\|v_1\|_{L^2(T)} \leqslant h_T \|\nabla v_1\|_{L^2(T)}$. Utilizing this, (5.10), and the definition of ρ_j in (5.11) results in

$$\|\rho\|^2_{H_0(\mathrm{rot})+t^{-1}\cdot L^2} \leqslant t^{-2}\|\rho_0\|^2_{L^2(\Omega)} + \sum_{T\in\mathscr{T}} (2 + h_T^2)\|\nabla v_1\|^2_{L^2(T)} \leqslant \frac{c_8^2}{t}\|h_{\mathscr{T}}^{1/2}\nabla_{\mathscr{T}}\rho\|^2_{L^2(\Omega)}. \tag{5.12}$$

The t-independent constant c_8 remains bounded as $h_{\mathscr{T}} \to 0$. □

Proof of Theorem 1. Combine Theorems 2, 4, and 6. □

Acknowledgements

The second author thankfully acknowledges partial support by the German Research Foundation (DFG) within the Graduiertenkolleg 'Effiziente Algorithmen und Mehrskalenmethoden'.

References

[1] D. Arnold, F.F. Brezzi, Some new elements for the Reissner–Mindlin plate model, in: J.L. Lions, C. Baiocchi (Eds.), Boundary Value Problems for Partial Differential Equations and Applications, Masson, Paris, 1989, pp. 287–292.
[2] D. Arnold, R. Falk, R. Winther, Preconditioning discrete approximations of the Reissner–Mindlin plate model, Math. Modell. Numer. Anal. 31 (1997) 517–557.
[3] D. Boffi, C. Lovadina, Analysis of new augmented Lagrangian formulations for mixed finite element schemes, Numer. Math. 75 (1997).
[4] D. Braess, Finite Elements, Cambridge University Press, Cambridge, MA, 1997.
[5] S. Brenner, L. Scott, The Mathematical Theory of Finite Element Methods, Texts in Applied Mathematics, vol. 15, Springer, New York, 1994.
[6] F. Brezzi, M. Fortin, Mixed and Hybrid Finite Element Methods, Springer, New York, 1991.
[7] F. Brezzi, D. Marini, E. Suli, Residual-free bubbles for advection-diffusion problems: the general error analysis, Numer. Math. 85 (2000) 31–47.
[8] C. Carstensen, Residual-based a posteriori error estimate for a nonconforming Reissner–Mindlin plate finite element, SIAM J. Numer. Anal., to appear.
[9] C. Carstensen, K. Weinberg, Calculating the energy-norm Fem-error for Reissner–Mindlin plates without known reference solution, Comput. Mech. 26 (2000) 566–570.
[10] P. Clément, Approximation by finite element functions using local regularization, RAIRO Sér. Rouge Anal. Numér. R-2 (1975) 77–84.
[11] D. Chapelle, R. Stenberg, An optimal low-order locking-free finite element method for Reissner–Mindlin plates, Math. Models Methods Appl. Sci. 8 (1998) 407–430.
[12] E. Liebermann, A posteriori error estimator for a mixed finite element method for Reissner–Mindlin plate, Math. Comput., to appear.
[13] C. Lovadina, A new class of finite elements for Reissner–Mindlin plates, SIAM J. Numer. Anal. 33 (1996) 2457–2467.
[14] L. Payne, H. Weinberger, An optimal Poincaré inequality for convex domains, Arch. Rat. Mech. Anal. 5 (1960) 286–292.
[15] L. Tartar, Remarks on some interpolation spaces, in: J.L. Lions, C. Baiocchi (Eds.), Boundary Value Problems for Partial Differential Equations and Applications, Masson, Paris, 1993, pp. 229–252.
[16] S.T. Timoshenko, J.N. Goodier, Theory of Elasticity, third ed., McGraw-Hill, New York, 1970.
[17] R. Verfürth, A Review of a posteriori Error Estimation and Adaptive Mesh-refinement Techniques, Wiley/Teubner, New York/Stuttgart, 1996.
[18] K. Weinberg, An adaptive finite element approach for a mixed Reissner–Mindlin plate formulation, Berichtsreihe des Mathematischen Seminars, Christian-Albrechts-Universität zu Kiel, Technical Report 22-99, 1999, http://www.numerik.uni-kiel.de/reports/1999/99-22.html.